

Scale-MIA: A Scalable Model Inversion Attack against Secure Federated Learning via Latent Space Reconstruction

Shanghao Shi*, Ning Wang[†], Yang Xiao[‡], Chaoyu Zhang*, Yi Shi*, Y.Thomas Hou*, Wenjing Lou*

^{*}Virginia Polytechnic Institute and State University, VA, USA

{shanghaos, chaoyu, yshi, thou, wjlou}@vt.edu

[†]University of South Florida, FL, USA

{ningw}@usf.edu

[‡]University of Kentucky, KY, USA

{xiaoy}@uky.edu

Abstract—Federated learning is known for its capability to safeguard participants’ data privacy. However, recently emerged model inversion attacks (MIAs) have shown that a malicious parameter server can reconstruct individual users’ local data samples through model updates. The state-of-the-art attacks either rely on computation-intensive search-based optimization processes to recover each input batch, making scaling difficult, or they involve the malicious parameter server adding extra modules before the global model architecture, rendering the attacks too conspicuous and easily detectable.

To overcome these limitations, we propose Scale-MIA, a novel MIA capable of efficiently and accurately recovering training samples of clients from the aggregated updates, even when the system is under the protection of a robust secure aggregation protocol. Unlike existing approaches treating models as black boxes, Scale-MIA recognizes the importance of the intricate architecture and inner workings of machine learning models. It identifies the latent space as the critical layer for breaching privacy and decomposes the complex recovery task into an innovative two-step process to reduce computation complexity. The first step involves reconstructing the latent space representations (LSRs) from the aggregated model updates using a closed-form inversion mechanism, leveraging specially crafted adversarial linear layers. In the second step, the whole input batches are recovered from the LSRs by feeding them into a fine-tuned generative decoder.

We implemented Scale-MIA on multiple commonly used machine learning models and conducted comprehensive experiments across various settings. The results demonstrate that Scale-MIA achieves excellent recovery performance on different datasets, exhibiting high reconstruction rates, accuracy, and attack efficiency on a larger scale compared to state-of-the-art MIAs.

Index Terms—Federated Learning, Secure Aggregation, Privacy Leakage, Model Inversion Attack.

1. Introduction

Federated learning (FL) is a distributed learning framework that enables its participants to collaboratively train

a machine learning model without sharing their individual datasets [1]. Within this framework, the training process occurs iteratively between a central parameter server and a group of clients. During each training round, the parameter server first broadcasts a global model with a pre-agreed model architecture to all or a fraction of clients. The server then collects and aggregates the model updates (gradient or parameter updates) submitted by the clients, which are trained and derived from their respective local datasets. As no individual training data samples are exchanged between participants in this process, federated learning is widely recognized as a communication-efficient and privacy-preserving learning paradigm.

1.1. Privacy Leakage of Federated Learning

Unfortunately, recent research reveals that the privacy of FL is susceptible to breaches, enabling attackers to infer information about clients’ proprietary datasets [2]. Of particular concern are the *model inversion attacks (MIAs or gradient inversion attacks)* [3], [4], [5], [6], [7], [8], [9], in which the adversary tries to reconstruct the original client training data from the model updates submitted by the clients. In these attacks, *the parameter server is considered an honest-but-curious attacker* whose goal is to closely approximate the input samples by minimizing the distance between real gradients uploaded by an individual client and those generated by approximated dummy samples. These attacks can successfully reconstruct high-fidelity input images when the server gains access to individual model updates and undergoes sufficient optimization iterations.

To counter these attacks, Bonawitz et al. propose the *secure aggregation (SA) protocol* [10] to prevent the server from gaining knowledge about individual model updates. Secure aggregation is a specialized secure multi-party computation (MPC) protocol that allows clients to securely compute the summation of model updates without exposing individual values. As a result, SA ensures that the parameter server can only know the aggregated model updates and is mathematically unable to distinguish individual updates from random numbers. SA is considered one of the most robust de-

fense mechanisms against various inference attacks targeting federated learning systems [11], and several follow-up works have been proposed to further reduce the communication and computation overhead of the original SA protocol [12], [13], [14], [15].

Unfortunately, recent development in privacy attacks shows that the SA protocol is breakable when the attacker is able to modify the model parameters or architectures, which *goes beyond the honest-but-curious threat model*. Two distinct attack strategies have been identified to break the SA protocol. The first strategy involves obtaining individual model updates (gradients) or their approximations from the aggregated results by carefully manipulating the global model parameters and having the gradients of the target client dominate the aggregated result. This can be achieved by eliminating the gradients of all other clients except the target [16], or amplifying only the gradients of the target victim [17]. The attacker then utilizes the individual gradients to perform gradient inversion attacks, attempting to reconstruct the original inputs. The limitation of these attacks is that they still require the costly per-input batch optimization process as part of the gradient inversion step. The second strategy involves a more direct approach to reconstructing the inputs from the aggregated results. To accomplish this, existing work requires the attacker to insert either a two-layer linear module [18] or a convolutional module [19] before the pre-agreed global model architecture, as well as possessing an auxiliary dataset. These modules are meticulously crafted or trained using the auxiliary dataset, enabling the attacker to reconstruct the inputs from the gradients of layers within these modules, using customized analytical methods when receiving local updates from the clients. However, this approach of modifying the pre-agreed model architecture is highly conspicuous and is unlikely to be accepted by the clients.

1.2. Our Attack

In this paper, we present a novel and robust model inversion attack named Scale-MIA, designed to be scalable, efficient, and highly effective. Scale-MIA is capable of recovering a large batch of inputs directly from the aggregated results, even if the SA protocol is in place. Notably, Scale-MIA is stealthy, requiring no modifications to the pre-agreed model architecture. Our attack strategy eliminates the need for a costly per batch or sample search-based optimization process, resulting in significant computational speed-up while achieving accurate data retrieval.

A key reason behind the high computation complexity in existing MIA works is that they treat machine-learning models as black boxes. To design a more efficient attack, we delve into the architecture of machine learning models and focus on the *latent space*, which corresponds to the layer right after the convolutional modules (e.g., AlexNet, VGGNet) and vision transformer (ViT) modules. We identify this layer as the most critical component for realizing efficient gradient inversion, given that it serves as the fundamental “information bottleneck” of the entire model architecture.

Similar to a typical machine learning system that comprises a training phase and an inference phase, the proposed Scale-MIA also involves two distinct phases—the *adversarial model generation* phase and the actual *input reconstruction* phase. The adversarial model generation can be done offline by the attacker, i.e., malicious parameter server, and it only needs to be done once at the outset. The purpose is to generate a crafted adversarial global model that the attacker will distribute to the clients during the FL iterations. To generate the adversarial model, the attacker first trains a surrogate autoencoder, with its encoder being identical to the encoder of the real global model, and a customized generative decoder capable of reconstructing the inputs, utilizing the collected auxiliary dataset. Subsequently, the attacker feeds the auxiliary dataset to the already-trained encoder, enabling the estimate of essential statistical parameters for crafting an adversarial global model. This adversarial global model follows exactly the same architecture as the pre-agreed model architecture and serves as a crucial component to facilitate the actual inversion attack in the second phase.

In the second phase, the attacker disseminates the crafted adversarial global model to the clients and awaits local updates from them. Assuming the presence of the secure aggregation (SA) protocol, the attacker only receives the aggregated gradients (model updates) from these clients. The proposed input reconstruction method takes the aggregated gradients (model updates) as input and aims to recover as many original inputs as possible. To significantly reduce the complexity of the inversion attacks, we design a novel gradient inversion method, in which we decompose the reconstruction phase into a two-step recovery process, each with much lower computation complexity. We first disaggregate the received local model update into batched latent space representations (LSRs) through a closed-form “linear leakage” module and then feed these representations into the pre-trained generative decoder to recover the original input batch. As both recovery steps only involve linear-complexity operations, the overall inversion process becomes super efficient to conduct. Note the attack phase can be executed in a single federated learning round and is adaptable for launch at any desired time.

Three factors could significantly impact the performance of Scale-MIA—The batch size that Scale-MIA can recover depends on the number of neurons in the first linear layer of the target model, the recovery accuracy is sensitive to the quantity and quality of the auxiliary dataset, and the recovery rate relies on the availability of a good statistical estimation of the distribution of LSRs. Unfortunately, in practical scenarios, the first and third factors do not pose a significant barrier for the attacker. Popular machine-learning models commonly feature large linear layers and real-world data often follows a Gaussian distribution, contributing to better attack performance. The data quality of the auxiliary dataset remains an uncertain factor. Nonetheless, the attacker can enhance attack performance by leveraging publicly available datasets or manually collecting samples relevant to its target. Our experiments demonstrate that the attacker can successfully execute a highly effective inference attack

using only open datasets or even just a few hundred targeted samples.

We conducted extensive experiments to evaluate the performance of the proposed Scale-MIA attack. A thorough comparison was made between our attack and existing MIAs using various image classification datasets, including Fashion MNIST (FMNIST) [20], CIFAR-10, and the skin cancer dataset (HMNIST) [21]. The results show a significant improvement in terms of attack accuracy, reconstruction fidelity, and efficiency when using Scale-MIA. We also evaluated Scale-MIA’s performance under different data settings, including variations in data amount and whether the data was iid or non-iid. The results consistently highlighted the success of Scale-MIA across all these settings. Particularly noteworthy is the results demonstrate that the attacker can effectively launch a targeted attack using his collected dataset over a specific class.

1.3. Contributions

This paper makes the following contributions:

- 1) Instead of treating the entire model as a black box, we delve into the internal architecture of machine-learning models and identify the latent space as the pivotal layer for launching a privacy inference attack. This insight motivates us to focus on the privacy risks posed by individual components within the model architecture, enabling us to devise a more efficient and effective attack strategy from a white-hat attacker’s perspective.
- 2) We propose Scale-MIA, a novel model inversion attack launched by a malicious parameter server. Scale-MIA efficiently and accurately recovers a large batch of inputs from the aggregated model updates, even if the federated learning system is under the protection of a robust secure aggregation protocol. Compared to existing attacks, Scale-MIA demonstrates significantly improved efficiency and scalability as it removes the requirement for expensive per-batch search-based optimization. Moreover, Scale-MIA is stealthier in its approach, as it does not require any modifications to the model architecture.
- 3) We provide a comprehensive analysis and evaluate the key factors that significantly impact the performance of Scale-MIA. Alongside our analysis, we present several practical attack scenarios for Scale-MIA to promote the need for novel defense mechanisms against such advanced attacks.
- 4) We conducted extensive experiments to evaluate the performance of Scale-MIA under diverse settings. We examined Scale-MIA’s performance on popular network architectures including Alexnet, VGGnet, ResNet, and ViT, as well as using various datasets. The results clearly show the effectiveness, efficiency, and scalability of our attack under various settings.

In Table 1, we summarize the definitions and notations used in our paper.

2. Background and Related Work

2.1. Gradient Inversion

Optimization-based Gradient Inversion: Federated learning allows participants to train a model collaboratively by only sharing their local model gradients or updates. However, recent research has revealed that an attacker can revert the gradient g_i uploaded by individual clients $i \in \{1, 2, \dots, n\}$ to their respective local datasets D_i by solving the following optimization problem:

$$\arg \min_{\hat{D}_i} [d(\nabla \hat{D}_i - \nabla D_i) + r(\hat{D}_i)] \quad (1)$$

where \hat{D}_i refers to the randomly initialized dummy samples, $d()$ refers to the distance function, and $r()$ refers to the regulation function. Zhu et al. [3] first identify this problem, and propose the deep leakage from gradient (DLG) attack which chooses the second norm as the distance function, and uses the L-BFGS optimizer [22] to solve the optimization problem. Zhao et al. [4] find that the DLG attack does not always achieve convergence or return the ground-truth labels consistently. Therefore, the paper proposes an improved version of the DLG attack by first recovering the ground-truth label from the gradients with an analytical method and then reconstructing the original images with higher confidence. Geiping et al. [5] further improve the optimization tool and achieve better image reconstruction fidelity, but requires a strong assumption as the labels of the inputs must be known. Yin et al. [7] focus on reconstructing batched inputs instead of individual ones on the ImageNet dataset and ResNet model architecture, making the attack more practical. Hatamizadeh et al. [9] customize the attack for the vision transformer and achieve better performance than previous attacks. However, these optimization-based gradient inversion attacks are computationally costly and need hundreds of optimization iterations to reconstruct one input batch [11]. Many of them (e.g., [3], [4], [5], [9]) only perform well for a single or small batch of images (typically smaller than 16), representing a scalability challenge.

Closed-form Gradient Inversion: Instead of the costly optimization approach that may take many iterations, another line of gradient inversion attacks seeks to reconstruct the input by closed-form derivation. Aono et al. [23] analyze the privacy leakage of the linear models and show that the inputs to the linear layers can be perfectly reconstructed from the gradients, which is referred to as the “linear leakage”. Many papers leverage this primitive as a component of their attacks [18], [17], [19]. We also use it as a component of our attack (more details in Section 3). Zhu et al. [6] propose an analytical recursive attack on privacy (R-GAP) to reconstruct the input layer by layer back from the output layer, particularly targeting linear and convolutional neural networks (CNNs). Lu et al. [8] propose an analytical reconstruction attack specialized for the vision transformer (ViT) and can reconstruct high-fidelity images. But unfortunately, each of these analytical attacks is only designed for its own model architecture and cannot be generalized for others.

TABLE 1. DEFINITION AND NOTATIONS.

Symbol	Definition
PS	Parameter server
c_i	Federated learning clients
n	Number of federated learning clients
G	Global model
θ	Global model parameters
t	Training round
m	Input batch size
D_i	Local dataset
g_i	Individual gradients
u_i	Masked individual gradients
SA	Secure Aggregation
x_i	Input samples
\hat{x}_i	Reconstructed samples
L	Loss function
D_{Adv}	Auxiliary dataset
G_{Adv}	Adversarial model
Enc	Encoder
MLP	Multi-layer perception
\hat{Enc}	Surrogate encoder
\hat{Dec}	Generative decoder
LSR	Latent space representations

Furthermore, they only perform well when assuming the reconstruction size is small.

2.2. Secure Aggregation

Previous gradient inversion attacks rely on the assumption that the attacker (i.e., the parameter server) can obtain the individual gradients $\{g_i\}$ from clients, especially for cross-device federated learning where each client is required to share gradients with the parameter server or other clients. As a countermeasure, Bonawitz et al. [10] propose the secure aggregation (SA) protocol that masks the original gradients from clients. Specifically, SA is a multi-party computation (MPC) protocol that masks the original model update (gradient) g_i with random bits u_i from secret sharing but keeps the summation of masked updates $\sum_{i=1}^n u_i$ identical to $\sum_{i=1}^n g_i$. Mathematically, this can be defined as:

$$f^{SA}(g_1, g_2, \dots, g_n) = (u_1, u_2, \dots, u_n) \quad (2)$$

$$s.t. \sum_{i=1}^n u_i = \sum_{i=1}^n g_i$$

where f^{SA} refers to the abstract function of the SA protocol and the attacker cannot distinguish u_i from a random number. This implies that nothing more than the final aggregated results is leaked to the attacker. Because the final results are aggregated from all training samples submitted by all participants, it is considered a large enough batch that is beyond the capability of previous gradient inversion attacks. The SA protocol also has other properties such as communication efficiency and drop-out resilience, making it one of the most robust defense mechanisms against the federated learning privacy inference attacks. The follow-up works further improve the performance of the original SA protocol by reducing the communication and computation overheads

[12], [24], [13], [14], enabling verifiable aggregation [15], and bolstering the robustness of the secure aggregation against malicious attacks [25], [26].

2.3. Breaking the SA

Although SA is designed to prevent the parameter server from knowing the individual gradients, recent work shows that the malicious parameter server can still recover the inputs just from the aggregated results. We classify the attacks against SA into two types including gradient disaggregation attacks and large batch reconstruction attacks.

Gradient Disaggregation Attacks: This type of attack seeks to overturn SA’s main function by inferring the individual gradients (i.e., before SA) from the aggregated results. To achieve this, Wen et al. [17] propose a “fishing strategy” that magnifies the gradient of a targeted class to dominate the aggregated result by crafting the model parameters. The attack aims to generate a close-enough approximation of the individual gradients out of the final aggregated gradients, which is enough for the attacker to reconstruct the original images through existing optimization-based gradient inversion attacks. Pasquini et al. [16] propose a gradient suppression attack that zeros out all the gradient updates except the target victim’s, making the final aggregated result identical to the gradient of the target client. The attack achieves this by crafting the parameters of a single linear layer and keeping the outputs of that specific layer to be always smaller than zero, which further leads to zero gradients if the ReLU activation function is used. Although the gradient disaggregation attacks can successfully break the SA protocol, they usually serve as the prerequisite attack to launch the gradient inversion attacks and are subject to the costly optimization overhead introduced by inversion steps. Moreover, this type of attack intrinsically assumes the batch size for calculating each gradient update is small, which may, unfortunately, violate the settings of some application scenarios such as for cross-silo federated learning.

Large Batch Reconstruction Attacks: Another attack strategy to break the SA is to directly reconstruct the whole input batch from the final aggregated results, treating the SA as a black box. This is a challenging problem and the existing attacks [18], [19] have strong assumptions to accomplish it, including letting the attacker modify the pre-agreed model architecture and possessing an auxiliary dataset that has a similar distribution as the clients’ training dataset. Fowl et al. [18] propose to attach an extra module of two linear layers to the pre-agreed architecture with adversarial parameters generated from the statistical information of the auxiliary dataset and the global batch size information. By customizing the extra module, the attacker can leverage the “linear leakage” primitive to perfectly reconstruct the original inputs with arbitrarily large batch sizes. Zhao et al. [19] improve this attack by adding a convolutional module before the original model architecture. By doing this the attacker can recover a larger batch of inputs with a smaller number of attack module parameters and support non-iid data settings. The key drawback of these attacks is that they require the

attacker to either change the pre-agreed model architecture significantly during the training time or force the participants to agree on the model architecture he desires before, which is an overly strong assumption in practice.

We summarize the pros and cons of existing attacks in Table 2. We compare the existing attacks with our proposed attack with respect to the attack assumption, overhead, and performance. Notably, our proposed Scale-MIA *scales significantly better* than the existing optimization-based gradient inversion attacks [3], [4], [5], [7], [9], [8] along with a *small attack overhead*, being *model-agnostic*, and the ability to launch a *targeted attack* against a certain class. Compare to the gradient disaggregation attacks [17], [16], Scale-MIA does not involve any per-batch optimization process and thus reduces the attack overhead (Scale-MIA can actually be used to replace the costly optimization-based inversion process after the individual gradient is obtained). Compared to the existing large-batch reconstruction attacks [18], [19], Scale-MIA assumes weaker attacker capability and is more stealthy and hard to detect.

3. Attack Preliminaries

3.1. Federated Learning

Federated learning (FL) allows a set of clients $\mathcal{C} = \{c_1, c_2, \dots, c_n\}$ to train a global model $G = f_\theta : \mathcal{X} \rightarrow \mathcal{Y}$ on a global dataset $\mathcal{D} = \cup_{i=1}^n D_i$ that is distributed along the users where each client c_i holds a local dataset D_i without the need to share these data samples. As a prerequisite, the model architecture of the global model G is pre-agreed by the participants including the parameter server S and the clients so that the clients can perform local training on the model with their datasets. FL is conducted iteratively in rounds until the model parameter θ converges. In each round t , the parameter server S first publishes the global model parameter θ^t to a subset of selected clients $\mathcal{C}^t \subseteq \mathcal{C}$. Then these clients compute model updates such as the gradients with their local batches D_i^t as $g_i = \frac{1}{|D_i^t|} \nabla L(\theta^t, D_i^t)$, where $L()$ refers to the loss function. The clients send their computed updates back to S and the latter will aggregate the updates with the FedSGD algorithm [1]:

$$\theta^{t+1} = \theta^t - \eta \sum_{i:c_i \in \mathcal{C}^t} \frac{\alpha_i}{|D_i^t|} \nabla L(\theta^t, D_i^t) \quad (3)$$

where η is the learning rate and α_i is the weight assigned to client c_i . The summation of all weights $\{\alpha_i\}_{i:c_i \in \mathcal{C}^t}$ is 1 and can be adjusted according to the number of data samples in different clients to avoid training bias on certain clients. The equation shows that there are two aggregation phases involved in the training procedure including the local aggregation among all samples when each client calculates the gradient and the global aggregation over the gradients from all clients. Conceptually, the FL process can be viewed as a gradient descent process on an abstract global training batch containing all samples in the local batches, i.e., $D_G^t = \cup_{i:c_i \in \mathcal{C}^t} D_i^t$. Besides FedSGD, the FL system may

also employ the FedAVG algorithm to conduct the training process (see Appendix). In the following sections, we will omit the notation t because our attack is a single-round attack and can be launched in any FL training round.

3.2. Autoencoder

Autoencoder is an unsupervised learning technique that helps to learn an informative and compressed representation of the data [27]. The autoencoder's model contains an encoder Enc and a decoder Dec . It is trained to minimize the difference between the original inputs and the reconstructed outputs, i.e., $\arg \min_{\theta} d(x, Dec(Enc(x)))$, where θ is the autoencoder's parameter vector and $d()$ refers to the error function such as the mean square error. Autoencoders are widely used in many applications such as dimension reduction, classification, clustering, anomaly detection, etc. [28], [29], [30], [31]. For our attack, we are leveraging the reconstruction capability of the autoencoder, which means for a given encoder architecture it is able to construct a decoder and train the decoder together with the encoder to generate highly similar outputs with the original inputs.

3.3. Linear Leakage

Considering a linear module with two linear layers and one non-linear activation function in between, linear leakage refers to the property that attackers can mathematically recover the batched inputs to this module from the aggregated gradients when the parameters of this module are carefully crafted and they know the cumulative density function (CDF) of one feature of the input data [18]. Here the recovery refers to the analytical or exact recovery without involving any estimation or approximation process. To describe this property, we first define the linear module as:

$$\begin{aligned} y &= \delta(w_1 x + b_1) \\ z &= w_2 y + b_2 \end{aligned} \quad (4)$$

where $x \in \mathbb{R}^d$, $y \in \mathbb{R}^k$, $z \in \mathbb{R}^o$, $w_1 \in \mathbb{R}^{k \times d}$, $b_1 \in \mathbb{R}^k$, $w_2 \in \mathbb{R}^{o \times k}$, $b_2 \in \mathbb{R}^o$, and δ is the ReLU function. Suppose the attacker knows the CDF of $h(x) = v_h \cdot x$ as $\psi(h(x))$, where $v_h \in \mathbb{R}^{1 \times h}$. Suppose the loss function is $L(x; \theta)$ or simply L where θ refers to the module parameters. Assuming the input batch size is m and the inputs can be expressed as $[x_1, x_2, \dots, x_m]$.

The attacker can reconstruct the inputs from the aggregated gradients by crafting the linear module as follows: (1) Having the row vectors $w_{1(i)}$ ($i = 1, 2, \dots, k$) of the weight matrix w_1 all identical to v_h ; (2) dividing the distribution of the feature $h(x)$ into equally k bins by calculating $h_i = \psi^{-1}(\frac{i}{k})$, which results in having a random h the same probability to falls in each bin $[h_i, h_{i+1}]$; (3) assigning the bias vector b_1 identical to the opposite values of the h vector $[-h_1, -h_2, \dots, -h_k]$; and (4) letting the row vectors of the weight matrix w_2 be identical.

TABLE 2. A COMPARISON BETWEEN DIFFERENT FEDERATED LEARNING MODEL INVERSION ATTACKS.

Attack	Break Secure Aggregation?	Attacker's Capability	Attack Overhead	Attack Scale	Need Auxiliary Dataset?	Model Agnostic?
DLG [3], iDLG [4]	No	Weak (Curious)	Large	Single image	No	Yes
Inverting Grad [5]	No	Weak (Curious)	Large	8	No	Yes
GradInversion [7]	No	Weak (Curious)	Large	48	No	No (ResNet)
GradViT [9]	No	Weak (Curious)	Large	8	No	No (ViT)
APRIL-Optim [8]	No	Weak (Curious)	Large	Single-image	No	No (ViT)
APRIL-Analytic [8]	No	Weak (Curious)	Small	Single-image	No	No (ViT)
R-GAP [6]	No	Weak (Curious)	Small	Single-image	No	Yes
Fishing for data [17]	Yes	Medium (Modify params)	Large	256	Yes	Yes
Eluding SecureAgg [16]	Yes	Medium (Modify params)	Large	512	Yes	Yes
Robbing the fed [18]	Yes	Strong (Change architect)	Small	1024	Yes	Yes
MANDRAKE [19]	Yes	Strong (Change architect)	Small	1024	Yes	Yes
Scale-MIA	Yes	Medium (Modify params)	Small	1024	Yes	Yes

As a result, the attacker recovers the input samples from the aggregated gradients by calculating the following equations for all $j \in (1, 2, \dots, k)$:

$$(\nabla_{w_1(j+1)}L - \nabla_{w_1(j)}L) / (\nabla_{b_1(j+1)}L - \nabla_{b_1(j)}L) \quad (5)$$

where specially we have $\nabla_{w_1(k+1)}L$ and $\nabla_{b_1(k+1)}L$ equal zero. Each sample in the input batch will activate and be recovered by one bin as long as the batch size m is smaller than k . More specifically, if one input sample x_p (i.e. the p^{th} smallest sample in terms of feature $h(x)$) falls in the l^{th} bin $[h_l, h_{l+1}]$ alone, the previous equation will produce the following results:

$$\begin{aligned}
\frac{\nabla_{w_1(l+1)}L - \nabla_{w_1(l)}L}{\nabla_{b_1(l+1)}L - \nabla_{b_1(l)}L} &= \frac{\frac{\partial L}{\partial y_{l+1}} \frac{\partial y_{(l+1)}}{\partial w_1(l+1)} - \frac{\partial L}{\partial y_l} \frac{\partial y_{(l)}}{\partial w_1(l)}}{\frac{\partial L}{\partial y_{l+1}} \frac{\partial y_{(l+1)}}{\partial b_1(l+1)} - \frac{\partial L}{\partial y_l} \frac{\partial y_{(l)}}{\partial b_1(l)}} \\
&= \frac{\sum_{v=1}^p \frac{\partial L}{\partial y_{l+1}} x_v - \sum_{v=1}^{p-1} \frac{\partial L}{\partial y_l} x_v}{\sum_{v=1}^p \frac{\partial L}{\partial y_{l+1}} - \sum_{v=1}^{p-1} \frac{\partial L}{\partial y_l}} \\
&= \frac{\sum_{v=1}^p \frac{\partial L}{\partial y_l} x_v - \sum_{v=1}^{p-1} \frac{\partial L}{\partial y_l} x_v}{\sum_{v=1}^p \frac{\partial L}{\partial y_l} - \sum_{v=1}^{p-1} \frac{\partial L}{\partial y_l}} \\
&= \frac{\frac{\partial L}{\partial y_l} x_p}{\frac{\partial L}{\partial y_l}} = x_p
\end{aligned} \quad (6)$$

Note that we have leveraged the property $\frac{\partial L}{\partial y_{l+1}} = \frac{\partial L}{\partial y_l}$. This is due to our assumption of having the row vectors of the weight matrix w_2 the same. More detailed discussions and proofs of Eq. (6) can be found in the appendix.

Linear Leakage Key Property: The above result shows that linear leakage is a powerful analytical tool to disaggregate the aggregated gradients in the linear layers and recover individual inputs from gradients. However, the number of bins k , which is also the number of neurons in the first linear layer, bottlenecks linear leakage's performance. In theory, linear leakage can at most recover an input batch with k

samples, otherwise, there will be collisions and the recovery of collided samples in one bin fails.

A straightforward attack strategy is to leverage the mathematical property of the "linear leakage" primitive and place a crafted linear module right in front of the global model G . As a result, when the gradients are back-propagated from the loss function to the linear module before G . It can precisely recover the inputs to it, which are exactly the inputs to model G . This is the fundamental idea of the current large batch reconstruction attacks [18], [19]. However, we consider this to be impractical in practice, especially for cross-silo federated learning where the participants have a certain power to verify the information provided by the server. It is too suspicious to have a linear module or its variants be attached before the global model G , especially when the FL system is designed for vision tasks and uses convolutional or vision transformer-based model architectures.

4. Threat Model

In this section, we formalize the attacker's capability and goal. We assume the parameter server is malicious and knows the global model G and its parameter θ of every round, as well as the aggregated gradient $\sum_{i=1}^n g_i$, where n is the number of participating clients. We consider the state-of-the-art SA protocol (as used in [10], [12]) is in place and the attacker only sees the already masked gradients $\{u_i\}_{i=1}^n$ from the clients rather than the original gradients $\{g_i\}_{i=1}^n$. The attacker cannot distinguish u_i from a random number but he can obtain the aggregated gradients $\sum_{i=1}^n g_i$ through summing the masked inputs $\sum_{i=1}^n g_i = \sum_{i=1}^n u_i$. We assume the communications between the parameter server and clients are secure and no third party can alter the transmitted messages between them. We assume the attacker is able to modify the global model G 's parameters but not architecture and knows all the training configurations such as the learning rate η and weights α_i , following the same attack assumptions as in [16] (CCS'22) and [17] (ICML'22). We also assume the attacker possesses an auxiliary dataset D_{Adv} as a subset of all the training data D_{Train} as in [18], [19]. The attacker can collect this D_{Adv} by using the

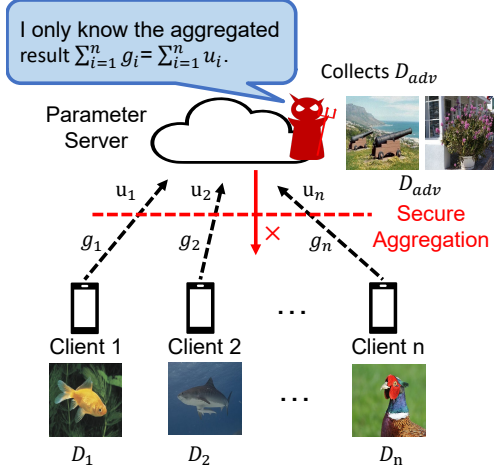


Figure 1. Scale-MIA threat model.

existing public datasets, manually collecting samples, or even colluding with a fraction of clients.

The attack aims to achieve the same goal as [18], [19], which is to recover the whole global input batch $\cup_{i=1}^n D_i$ efficiently and precisely. We illustrate our threat model in Figure 1.

5. Attack Method

5.1. Attack Intuition

Existing model inversion attacks against FL typically treat the global model G as a black box, which, unfortunately, introduces several attack limitations. Optimization-based inversion attacks attempt to reverse the gradient calculation or the learning process by iteratively feeding dummy inputs to the black box G to approximate the original inputs. However, this approach results in excessive computation overhead, as for each sample the attacker needs to reverse the model calculation once by solving a time-consuming search-based optimization problem. This approach also lacks a fundamental “disaggregation step” and the reversed results are usually still mixed together for batched inputs. More recent large-batch reconstruction attacks introduce a new angle by focusing on the input layers of G —a linear module is added in front of G and the linear leakage primitive is exploited to directly recover the inputs to the module, which is exactly the input samples. However, as we have discussed, the major drawback of this method is the addition of the extra module, which is highly suspicious and easily detectable by vigilant participants. For our attack, we strive to overcome these limitations and incorporate the following key properties to enhance its performance and efficiency:

- The new attack shall harness the advantageous mathematical properties of the linear leakage primitive to recover individual samples from the aggregated results, avoiding the recovered samples mixed together.

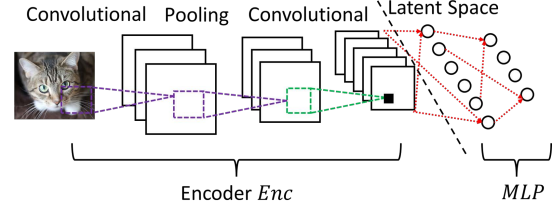


Figure 2. The model architecture of machine-learning classifiers.

- We aim to develop an attack strategy that manipulates only the model weights without making any changes to the model architecture.
- To ensure scalability for large batch reconstruction, our new attack shall only use efficient closed-form or feed-forward matrix computations during the attack phase, eliminating the need for costly search-based optimization steps.

To accomplish this, we take advantage of the architectural commonality in existing classifiers and decompose the inversion problem into sub-problems to reduce its difficulty and complexity. We noted that popular classifiers commonly feature a non-linear encoder Enc followed by a multi-layer perceptron (MLP), as exemplified in Figure 2 using a convolutional neural network. This observation motivates us to target the latent space as the key layer for Scale-MIA, as it is the “information bottleneck” of the entire architecture, preserving essential input data information while maintaining lower dimensions for efficient processing. In our approach, we decompose the inversion problem into two sub-problems—first recovering the LSRs from the aggregated gradients and subsequently recovering inputs from the LSRs. Fortunately, we can utilize the linear leakage primitive with the first two layers in the MLP to recover the LSRs. This is a closed-form solution that ensures both recovery accuracy and small linear computation complexity. For the second problem, we employ an autoencoder to train a generative decoder Dec to address it. This step also only involves the feed-forward matrix computation of neural networks with linear complexity after the generative decoder Dec is trained offline.

5.2. Attack Overview

We illustrate the attack flow of Scale-MIA in Figure 3. Scale-MIA consists of two main phases: the adversarial model generation (training) phase (Steps ①-④) and the input reconstruction (attack) phase (Steps ⑤-⑦). The first phase is conducted locally on the parameter server S and its purpose is to generate an adversarial global model G_{adv} with crafted parameters, as well as a highly accurate generative decoder \hat{Dec} . This phase starts with crafting a surrogate autoencoder \hat{A} that has the same encoder architecture Enc as the global model G ’s encoder Enc , and a customized decoder \hat{Dec} that has the capability to reconstruct the inputs. The attacker then trains \hat{A} with his own auxiliary dataset D_{Adv} . After training, the attacker feeds the auxiliary dataset D_{Adv} to the

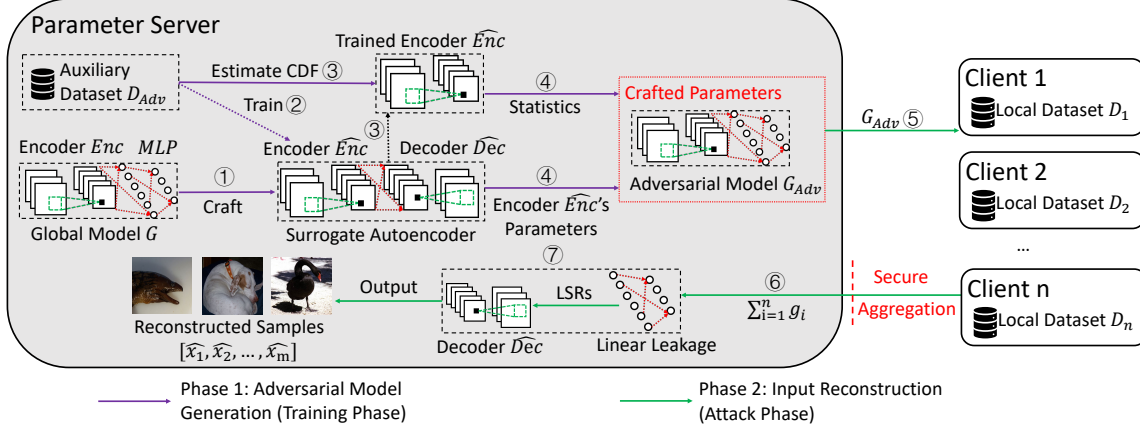


Figure 3. Scale-MIA is a two-phase attack. The first phase is performed locally to produce essential information to conduct the second phase. The second is the actual attack phase for the attacker to interact with the clients and reconstruct their sensitive samples.

already trained encoder and uses statistical methods to obtain necessary statistics for crafting the malicious global model G_{Adv} . The adversarial model G_{Adv} is crafted with both the parameters from the trained encoder and the estimated statistics. This phase is conducted completely offline and covers all the required training efforts.

For the input reconstruction phase, the attacker first distributes the adversarial model G_{Adv} to the clients and awaits their feedback. After receiving the feedback, the attacker examines the gradients of the MLP layers in the adversarial global model to first recover the batched latent space representations (LSRs) through the linear leakage primitive, and then reconstruct the input samples by feeding the LSRs to the trained decoder Dec . All the operations involved in this actual attack phase only involve linear-complexity calculations and the reconstruction is significantly accelerated.

5.3. Detailed Workflow

Adversarial Model Generation: We assume that the global model G has an architecture consisting of an encoder Enc followed by a multi-layer perception (MLP). This assumption is practical and commonly observed in popular image classification models such as CNN-based AlexNet, VGGNet, ResNet, and Vision Transformer. In step ①, the attacker crafts a surrogate autoencoder \hat{A} consisting of an encoder \hat{Enc} and a decoder \hat{Dec} . The encoder \hat{Enc} has the same model architecture as the global model’s encoder Enc and the decoder \hat{Dec} is constructed according to the model architecture of \hat{Enc} . For example, for an encoder that has several CNN layers, the decoder can have several de-convolutional layers to reconstruct the input. In step ②, the attacker trains the surrogate autoencoder \hat{A} using its own dataset D_{Adv} with the objective of minimizing the distance between its inputs and outputs. D_{Adv} can be a publicly available dataset or a custom-collected dataset targeting a specific purpose or victim. In step ③, the attacker feeds its dataset D_{Adv} to the already trained encoder \hat{Enc} to get

the LSRs LSR_{Adv} of the dataset. The attacker estimates the CDF of the brightness (the average value among all pixels) of the LSR_{Adv} and calculates the corresponding bias vector $H = [-h_1, -h_2, \dots, -h_k]$ of the k bins according to the “linear leakage” primitive we described. Here k is identical to the neuron number of the first MLP layer of the global model G . Finally, in step ④, the attacker modifies the adversarial global model G_{Adv} by having the parameters of G_{Adv} ’s encoder identical to \hat{Enc} and crafting a linear leakage module with the first two MLP layers with respect to H . More specifically, the attacker has all the elements of the weight matrix of the first layer w_1 identical to $\frac{1}{d}$, where d is the dimension of the LSRs; as well as having the bias vector of the first layer b_1 equals H and the row vectors of the second weight matrix w_2 identical.

Input Reconstruction: After generating the adversarial model G_{Adv} , the attacker publishes it in step ⑤ to all the clients. Then according to the FL framework, in step ⑥ the clients reply an aggregated gradient $\sum_{i=1}^n g_i$. In step ⑦, the reconstruction module takes the aggregated statistics as the input and first uses the linear leakage to recover a batch of latent space representations, i.e. $[LSR_1, LSR_2, \dots, LSR_m] = LinearLeak(\sum_{i=1}^n g_i)$, where m is the global batch size identical to the cardinality of $\bigcup_{i=1}^{|C|} D_i$. Then these LSRs are taken as the inputs to the trained decoder \hat{Dec} and the attacker finally gets $\hat{x}_j = \hat{Dec}(LSR_j) = \hat{Dec}(\hat{Enc}(x_j))$ for $j \in \{1, 2, \dots, m\}$ as the reconstruction outputs. According to the property of the autoencoder, for all $j \in \{1, 2, \dots, m\}$, \hat{x}_j and x_j are identical or highly similar.

5.4. Efficacy and Efficiency Analysis

Performance Bottleneck: There are three main factors that affect the performance of Scale-MIA. The first one is the neuron number of the first linear layer, denoted by k . This is because we adopt the linear leakage primitive as a component in our attack and therefore, our attack is subject to its constraints. Fortunately, the current neuron numbers of

the first linear layers of the popular machine learning models are very large, typically more than one thousand (typical numbers: 1024/4096), which is enough for the attacker to reconstruct hundreds of samples simultaneously. Ideally, the attacker can reconstruct an input batch with size k . But in practice, because of imperfect statistical estimation and data bias, this upper bound is never reached. In general, the larger the batch size is, the higher the probability there are collisions in the recovery bins. All collided images in a bin are mixed up and their recovery fails. In our experiment, we find that the attacker is able to recover images with a high recovery rate (≥ 0.6) when the batch size is smaller than half of the neuron number $\frac{k}{2}$.

The second factor is the quality of the auxiliary dataset D_{Adv} . D_{Adv} is used to train the surrogate autoencoder and estimate the essential statistics. In the ideal case, if the auxiliary dataset has the same distribution as the training dataset, the attacker can recover every sample in the training dataset. But in practice, there are usually data biases, and the auxiliary dataset cannot precisely represent the distribution of the training dataset. Fortunately, Scale-MIA enables the attacker to launch the targeted attack, which means even if the attacker cannot reconstruct all the samples with an amount-deficient and biased dataset, he can still infer a target class if there are enough data samples in that class. In other words, the attacker needs to collect as many data samples as possible for his target class, and the more he collects, the better the attack performs.

The third factor that affects the performance of Scale-MIA is whether the attacker can have a good estimation for the required CDF. The problem is whether the ground-truth CDF of the LSRs could be accurately estimated, for it may exhibit uncommon distributions and become hard to model and estimate. Fortunately, in our experiment, we find that the LSRs usually exhibit Gaussian or Laplace distribution and can be easily and accurately estimated.

Attack Overhead: The major overhead imposed by Scale-MIA is in the adversarial model generation phase, or more specifically, the training process of the autoencoder. Except this, the CDF estimation step and model crafting step only involve analytical operations and are efficient to be performed. Fortunately, Scale-MIA allows this phase to be conducted fully offline and the attacker can leverage any computation resource to fulfill this. The attacker can also resort to finding publicly available pre-trained autoencoders because there are many pre-trained autoencoders available on the Internet that cover most of the popular machine-learning models. The attacker can directly use them if the FL framework chooses the global models among these popular model architectures.

The input reconstruction phase (i.e., the attack phase) also only imposes very small overheads because this phase only requires closed-form matrix computation or feed-forward operations in already trained neural networks with linear complexity. A unique advantage of Scale-MIA is that the attacker can iteratively use the trained autoencoder to launch attacks for multiple rounds, i.e. “train once, and attack multiple rounds”. In our experiment, we will show that

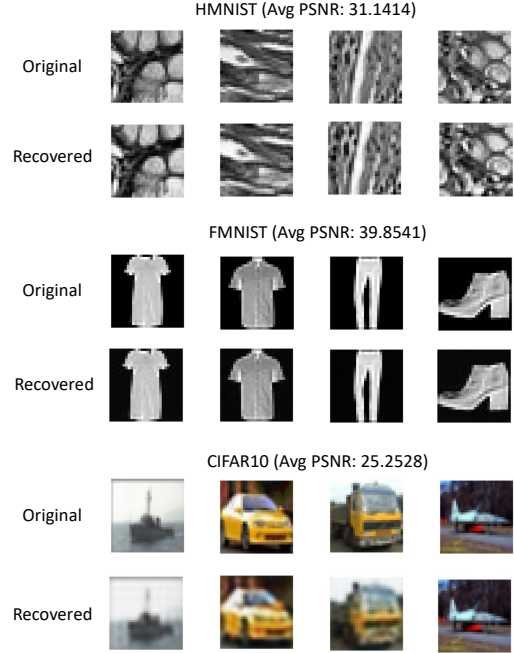


Figure 4. Reconstruction Examples. These examples are taken from a large reconstruction batch. Full recovered batches can be found in the appendix.

Scale-MIA’s computation time for reconstructing one batch of input is more than 100 times smaller than the current costly optimization-based model inversion attacks.

5.5. Practical Attack Scenarios

Large Batch Reconstruction: Scale-MIA enables the attacker to reconstruct a large batch of inputs simultaneously. To further improve the attack’s extendability to reconstruct different classes of data samples, the attacker can choose the large publicly available datasets as the auxiliary dataset. For example, the attacker can use the ImageNet dataset to train its autoencoder when he aims to recover images. The attacker may also train the autoencoder with a large medical dataset if he tries to recover some sensitive medical records.

Targeted Inference: Another attack strategy for the attacker is to collect data samples for a certain target class to launch the targeted attack. For example, the attacker wants to infer the images of the “dog” class. What he needs to do is collect samples with the label “dog” as many as possible. As a result, even if the attacker can not recover the other classes of images, he can still recover the images with the label “dog” precisely. In practice, this gives the attacker the ability to obtain sensitive information for a certain victim class such as inferring the records of a certain group of patients. In our experiment, we will show that this is very practical and the attacker only needs to collect several hundred samples in order to obtain a decent attack performance.

Enhance the Existing Attacks: Many of the existing privacy inference attacks, especially the gradient disaggregation attacks [18], [16] use the current optimization-based gradient inversion attacks as the final step to reconstruct the

TABLE 3. THE COMPARISON BETWEEN SCALE-MIA AND THE OTHER ATTACKS.

Attack	Model	Metric	1	2	4	8	16	64	256
DLG [3] /iDLG [4]	CNN	PSNR (dB)	23.6666	–	–	–	–	–	–
		Time (s)	117.3938	–	–	–	–	–	–
InvertingGrad [5]	Resnet	PSNR (dB)	25.7889	16.8597	15.8345	13.3967	–	–	–
		Time (s)	86.8926	81.2130	84.0691	84.2910	–	–	–
GradInversion [7]	Resnet	PSNR (dB)	15.3059	14.7896	14.0550	12.1410	11.1029	–	–
		Time (s)	324.8003	341.6113	348.2077	377.3184	462.2559	–	–
Fishing for User [17]	Resnet	PSNR (dB)	19.1928	15.7852	18.0432	17.4613	16.3979	17.4164	18.9252
		Time (s)	231.5289	285.4572	227.2872	285.8083	291.9067	285.0060	285.4065
Robbing the Fed [18]	Resnet	PSNR (dB)	161.0681	160.4941	120.5119	130.6829	133.4840	120.6985	84.3942
		Time (s)	0.1843	0.1877	0.1842	0.1843	0.1860	0.1994	0.2321
Scale-MIA	Resnet	PSNR (dB)	21.1686	22.4811	24.4638	26.5762	27.4551	27.9498	27.6572
		Time (s)	0.008613	0.008978	0.01013	0.01074	0.01418	0.03591	0.1311

inputs after the attacker obtains the individual gradients from the aggregated results. However, the individual gradients may still be an aggregated result with local batches and many of the existing attacks fail when the local batch size is large. They also suffer from the large computation overhead introduced by the costly iterative optimization rounds. Scale-MIA can be used to replace these attacks to enhance the disaggregation attacks, for Scale-MIA achieves better attack performance with significantly smaller attack overhead and larger attack scale.

6. Evaluation

6.1. Experiment Settings

We implemented Scale-MIA on the PyTorch platform. We run all the experiments on a server equipped with an Intel Core i7-8700K CPU 3.70GHz \times 12, a GeForce RTX 2080 Ti GPU, and Ubuntu 18.04.3 LTS. We considered three important metrics including the recovery batch size, recovery rate, and the peak signal-to-noise ratio (PSNR) score. The batch size refers to the global batch size, i.e. the cardinality of the union of all the local datasets $|\cup_{i=1}^n d_i|$. This can be interpreted as the multiplication of the local batch size and the number of clients n . For example, a global batch with 512 samples can be uploaded by 512 mobile clients with each client having one sample, by 16 clients with each having 32 samples, or just by one client with 512 samples. The recovery rate is the ratio between successfully recovered samples and the total samples. The definition of the successfulness of recovering a sample is by calculating the PSNR score between the original input sample and the reconstructed one, and checking whether the score exceeds a certain threshold th . In our work, we take $th = 18$ because this threshold is enough for the attacker to clearly distinguish the meaningful contents from the recovered figures. The PSNR score is a widely adopted metric to quantify reconstruction quality for images and video subject to lossy compression. It can be expressed as $PSNR = 20 \log_{10}(\frac{\max_I}{\sqrt{MSE}})$, where \max_I refers to the maximum image pixel value and MSE refers

to the mean square error. In this work, we use it to measure the performance of Scale-MIA, following the convention of the existing papers [5], [18], [17].

We implemented Scale-MIA on the Fashion MNIST (FMNIST) [20], Colorectal Histology MNIST (HMNIST) [21], and CIFAR-10 [32] datasets. FMNIST consists of a training set of 60,000 samples and a test set of 10,000 samples. Each sample is a 28×28 grayscale image, associated with a label from 10 classes, including T-shirt, trousers, pullover, dress, coat, sandal, shirt, sneakers, bag, and ankle boot. HMNIST is a medical dataset that contains 5000 images for 8 types of skin cancers. Each sample is a 28×28 grayscale image, associated with a label from 8 classes of cancers. The CIFAR-10 dataset consists of 60,000 32×32 color images in 10 classes, with 50,000 training images and 10,000 test images. Each image is from one of the ten classes, including airplane, automobile, bird, cat, deer, dog, frog, horse, ship, and truck. We evaluated Scale-MIA's performance on the popular model architectures including the convolutional neural network (CNN), AlexNet [33], VGGNet [34], ResNet [35], and ViT [36].

For each result, we repeated our experiment 5 times to eliminate uncertainty and noise. In Figure 4, we demonstrate several reconstructed examples over the three datasets. We plot the original images in the first row and the reconstructed ones in the second row along with the average PSNR score. More reconstruction figures with larger batch sizes and detailed model architectures can be found in the appendix.

6.2. Benchmark Comparison

We implemented and compared Scale-MIA with state-of-the-art model inversion attacks that have publicly available artifacts, including the DLG [3] /iDLG [4], GradInversion [7], Inverting Gradient [5], fishing for user [17], and robbing the fed [18] attacks. To make a fair comparison, we re-implemented all these attacks on the CIFAR-10 dataset and with the Resnet model architecture unless this setting is not supported, for which we took the CNN instead. We focused on the average PSNR score and attack time (the

TABLE 4. THE RECOVERY RATE OF SCALE-MIA OVER DIFFERENT MODELS AND BATCH SIZES.

Models	Datasets	64		128		256		512		1024	
		Rate	PSNR	Rate	PSNR	Rate	PSNR	Rate	PSNR	Rate	PSNR
Alexnet (512)	CIFAR-10	0.9146	29.0523	0.8383	28.8489	0.7308	28.5446	0.4974	27.2409	–	–
	FMNIST	0.8811	31.0618	0.8025	30.7896	0.6407	30.2081	0.4193	29.6587	–	–
	HMNIST	0.9150	28.7399	0.8691	28.6298	0.7598	27.5238	0.5313	23.5482	–	–
Resnet* (512)	CIFAR-10	0.9162	27.9498	0.8408	27.6572	0.7136	26.7230	0.4869	24.1208	–	–
	FMNIST	0.9050	26.8347	0.8289	26.8591	0.6841	26.5266	0.4469	25.0946	–	–
	HMNIST	0.8251	22.8118	0.7792	22.6694	0.6699	22.6648	0.2416	21.0613	–	–
ViT* (512)	CIFAR-10	0.6753	21.0227	0.6220	21.0034	0.5291	20.9522	0.2313	20.7623	–	–
	FMNIST	0.8533	24.6116	0.7739	24.5138	0.6607	24.3117	0.3958	23.7067	–	–
	HMNIST	0.7520	24.0052	0.7001	24.0819	0.6006	24.0337	0.4325	23.1862	–	–
CNN (1024)	CIFAR-10	0.9522	26.1183	0.9204	26.0259	0.8464	25.8141	0.7126	25.4831	0.4947	25.0468
	FMNIST	0.9493	38.4984	0.9146	38.1457	0.8229	37.7319	0.6844	36.3472	0.4775	34.1014
	HMNIST	0.9639	33.4123	0.8799	32.4604	0.7783	31.6734	0.7051	30.6976	0.4164	21.9814
VGG (1024)	CIFAR-10	0.9572	28.2689	0.9191	28.2333	0.8463	27.7959	0.7301	26.9002	0.5032	25.0889
	FMNIST	0.9426	29.5836	0.8977	29.5582	0.7954	29.1365	0.6485	28.2728	0.5630	28.9405
	HMNIST	0.7734	24.6297	0.7177	24.1802	0.6855	24.6799	0.6182	24.2040	0.4956	24.2747

time to recover one batch of inputs) metrics to evaluate the effectiveness and efficiency of the attacks on recovering sample batches whose sizes ranged from $\{1, 2, 4, 8, 16, 64, 256\}$. We summarize the attack results in Table 3.

From the experiment results, we observe that Scale-MIA outperforms all other attacks in terms of reconstruction accuracy, except the Robbing the fed attack [18], which achieves a super-high accuracy because it has the strongest assumptions among all attacks. We observe another interesting phenomenon: the average PSNR score for Scale-MIA increases as the batch size becomes larger, while all other attacks show the opposite trend. This may be because Scale-MIA is designed to recover large batches of inputs, and the impact of noise and uncertainty is exacerbated when the batch size is very small. The batch sizes we used in this experiment have reached or exceeded the performance upper bound of many attacks, but they have not yet reached the performance bottleneck of Scale-MIA. In the next section, we will show that when the batch size continues to increase, Scale-MIA’s performance will reach its bottleneck and decrease with respect to batch sizes, showing a similar trend with others.

In terms of attack efficiency, we observe that all the optimization-based model inversion attacks [3], [4], [5], [7], [17] require a significant amount of computational resources and can take hundreds of seconds to recover just one batch of inputs. As a comparison, the closed-form Robbing the Fed attack [18] and our proposed Scale-MIA are much more efficient, capable of completing the inversion process within milliseconds.

In terms of the attack scale, DLG [3] / iDLG [4], GradInversion [7], Inverting Gradient [5] attacks can only recover small batches with less than 16 samples. But fishing for user [17], robbing the fed [18], and our Scale-MIA can achieve stable performance when the attack scale is larger. Particularly, the robbing the fed [18] attack is a very powerful one as it achieved an even better PSNR score, and a similar level of attack efficiency performance on a large scale

compared to Scale-MIA. But as we have discussed before, this is due to this attack having a much stronger assumption—being able to significantly modify the pre-agreed model architecture, which Scale-MIA does not need.

6.3. Large Batch Recovery Performance

We implemented Scale-MIA on various model architectures, including convolutional neural network (CNN), AlexNet, VGGNet, ResNet, and ViT. Because the original Resnet and Vit only have a single linear layer after the encoder module, we mark an asterisk beside them, indicating that Scale-MIA only applies to their modified version with two linear layers. We evaluated Scale-MIA’s performance in terms of reconstruction rate and average PSNR score of the successfully recovered samples with respect to batch sizes ranging from $\{64, 128, 256, 512, 1024\}$ to validate Scale-MIA’s performance on recovering large batches. The experiment results are shown in Table 4.

From the results, we can see that in general Scale-MIA achieves high PSNR scores for all model architectures and batch sizes. There is no performance pitfall that leads to a significantly small PSNR score lower than our threshold, which means that all the successfully recovered samples are of good quality, even for very large input batches. Meanwhile, we observe that the recovery rate is monotonically decreasing with respect to larger batch sizes. This is reasonable and in line with our expectation, as larger recovery batches increase the probability of recovery collisions and failures. In Figure 5, we plot the PSNR distribution of four randomly selected batches with sizes $\{64, 128, 256, 512\}$ recovered by Alexnet on the CIFAR-10 dataset. It is clear that with larger batch sizes the PSNR distribution becomes worse and more recovered samples fall below the threshold $th = 18$.

We include the neuron number of the first linear layer k beside the model architecture and find that the recovery rate is largely affected by it. The models with larger k have

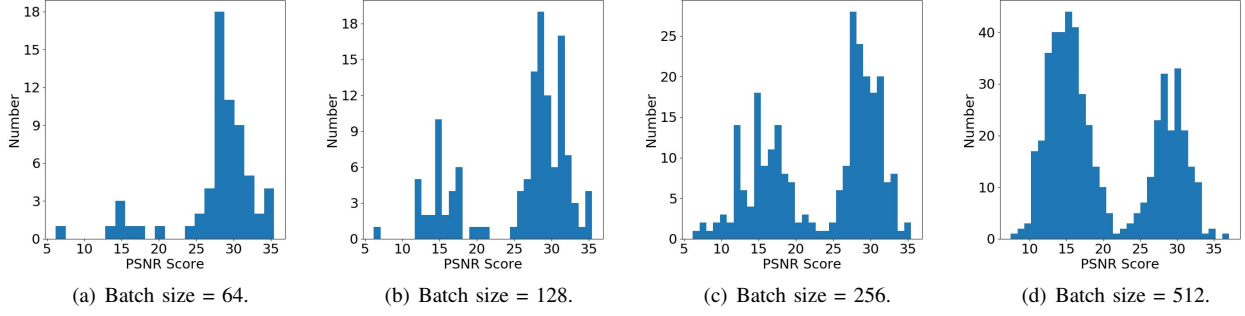


Figure 5. The PSNR distribution of different sizes of input batches for AlexNet on CIFAR-10.

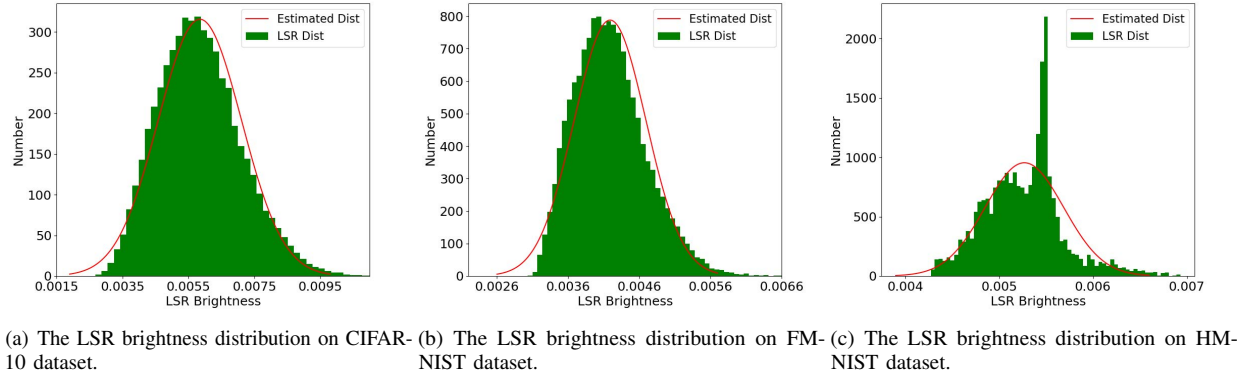


Figure 6. The LSR brightness distribution of different datasets for Alexnet and their estimation results.

better recovery rates for a fixed batch size except for a few outliers. We observe that Scale-MIA achieves good recovery rates when the batch sizes are smaller than half of the neuron number k .

In Figure 6, we show the LSR brightness distribution on different datasets where the LSRs are generated by feeding the datasets to the trained surrogate encoder Enc . We observe that the LSR distribution of the CIFAR-10 and FMNIST datasets are highly similar to the Gaussian distribution and are easier to estimate. However, we notice a high peak in the distribution of the HMNIST dataset, which indicates its estimation is unstable. This can be verified by checking the recovery rate performance of ViT, Resnet, and VGG, for in these cases, the recovery rate of HMNIST is significantly smaller than the other two datasets. We consider this to be because of the intrinsic data bias of HMNIST. Compared to CIFAR-10 and FMNIST, HMNIST is much smaller to have only 5000 samples and some of its features may not follow the Gaussian distribution as most of the large datasets do. This leads to unstable and imperfect distribution estimation and finally affects the attack performance.

6.4. Data Deficiency and Bias

The quality of the auxiliary dataset D_{Adv} is an important factor that impacts the performance of Scale-MIA. The ideal

situation is that D_{Adv} has the same distribution and can represent the training dataset well. However, in practice, there is usually data deficiency and bias and we evaluate the impacts of them in this section.

Data Deficiency: We varied the amount of data available to the attacker for launching Scale-MIA and evaluated its performance on the CIFAR-10 dataset using the AlexNet model. We considered scenarios where the attacker possesses different proportions of the total training data, ranging from 1% to 100% (equivalent to 500 to 50,000 images). The attack performance was tested on the entire validation set, which consists of 10,000 images. Given that the first linear layer of the AlexNet model has 512 neurons, we varied the recovery batch size from 16 to 256 to ensure a reasonable recovery performance of Scale-MIA.

Table 5 and Table 6 shows the recovery rate and PSNR score of Scale-MIA under various data settings, respectively. We observe that the number of samples available to the attacker has very little impact on the recovery rate, as it remains relatively stable at high values across the full range of data availability. The PSNR score does decrease slightly when the number of samples decreases, but it remains to be in a decent range. Specifically, even if the attacker only has 1% samples (500 images) of the training dataset, Scale-MIA still achieves very high recovery rates and PSNR scores in

TABLE 5. THE RECOVERY RATE OF SCALE-MIA OVER DIFFERENT AMOUNTS OF DATA.

Batch/Amount	1%	3%	10%	100%
16	0.9808	0.9824	0.9809	0.9827
32	0.9537	0.9569	0.9550	0.9586
64	0.9090	0.9136	0.9143	0.9146
128	0.8243	0.8316	0.8317	0.8383
256	0.6873	0.6923	0.7018	0.7308

TABLE 6. THE PSNR SCORE OF SCALE-MIA OVER DIFFERENT AMOUNTS OF DATA.

Batch/Amount	1%	3%	10%	100%
16	25.1174	25.4396	27.9021	29.4134
32	24.9192	25.2514	27.7217	29.1968
64	24.8604	25.1489	27.6032	29.0523
128	24.6688	24.9584	27.3481	28.8489
256	24.3534	24.6209	26.8835	27.2409

our experiment. This indicates that Scale-MIA is a practical attack and the attacker only needs to collect or generate a few hundred samples to obtain a decent attack performance.

Data Bias: We assumed the attacker had access to different numbers of data classes from the CIFAR-10 dataset to evaluate Scale-MIA’s performance over biased data. We considered the attacker to have $\{1,2,3,10\}$ classes of data samples and evaluated Scale-MIA’s performance on these particular classes. For example, if we had the attacker possess the “dog” samples, we would only evaluate Scale-MIA’s performance on recovering the “dog” samples in the validation set. We continued to focus on the PSNR score and recovery rate for batch sizes ranging from 16 to 256.

Table 7 and Table 8 present the targeted attack’s performance. The results show that data bias has a very limited impact on the recovery rate, as it remains stable even when the attacker has only a few classes of samples. The decrease in PSNR score is also not significant, and even the worst value remains at a high level. These results demonstrate that Scale-MIA’s attack performance is robust against data bias. The attacker can successfully launch a targeted attack on specific classes with minimal performance degradation.

7. Discussion

Differential Privacy: Differential privacy (DP) [37] has been widely used to protect training data privacy in machine learning systems recently [38], [39]. It has shown its effectiveness in protecting client-level and data record-level membership privacy for FL systems [39] by preventing the attacker from knowing whether one item (a client or a record) exists in the system. Though DP can protect the FL system against membership inference attacks by its definition, it is demonstrated less effective against data reconstruction attacks [40]. Scale-MIA, categorized as a data reconstruction attack, is expected to break DP as well. We defer the analysis of the (in)effectiveness of DP in Scale-MIA to future research.

Targeted Attack: In section 5, we discuss how to launch a targeted model inversion attack against a targeted class.

TABLE 7. THE RECOVERY RATE OF SCALE-MIA OVER DIFFERENT NUMBERS OF CLASSES OF DATA.

Batch/Amount	1	2	3	10
16	0.9818	0.9856	0.9753	0.9827
32	0.9557	0.9701	0.9505	0.9586
64	0.8984	0.9128	0.8971	0.9146
128	0.8307	0.8568	0.8229	0.8313
256	0.6914	0.7214	0.6615	0.7308

TABLE 8. THE PSNR SCORE OF SCALE-MIA OVER DIFFERENT NUMBERS OF CLASSES OF DATA.

Batch/Amount	1	2	3	10
16	25.1320	24.8238	25.2728	29.4134
32	25.0041	24.8306	25.2147	29.1968
64	24.8337	24.7875	25.1607	29.0523
128	24.5928	24.5584	25.0155	28.8489
256	24.1795	24.0819	24.5275	27.2409

However, in many situations, the attacker is more curious about sensitive information for a certain client. Scale-MIA cannot accomplish this even if it can recover the whole batch in high fidelity because the attacker cannot tell which recovered sample is from whom when SA protocol is in place. This is referred to as the “privacy by shuffling” property of the SA protocol [16]. To break this, Scale-MIA needs to be used in conjunction with the gradient disaggregation attacks [17], [16] by letting them first obtain the individual gradients from the victims and then using Scale-MIA as an enhancement to recover samples.

Two-Linear-Layer Limitation: Scale-MIA takes the “linear leakage” as its component, and as a result, it requires the model to have two consecutive linear layers. Although most of the existing model architectures have this module, some Resnet-based and ViT-based models do not. To conduct Scale-MIA on these models, the attacker must have stronger capabilities to add an extra linear layer at the end of the model. Meanwhile, we observe that the ViT model contains built-in linear layers within its *Enc* module. We leave this as our future work to investigate whether these linear layers outside the latent space can leak private information.

8. Conclusion

In this paper, we propose Scale-MIA, a powerful MIA that breaks the strong SA mechanism by reconstructing the whole global batch simultaneously in an efficient manner. Scale-MIA launches the model inversion attack from a new angle by not treating the targeted model as a black box and decomposing the inversion problem in two steps including a LSR recovering step and an input generation step. Scale-MIA uses the closed-form “linear leakage” primitive to conduct the first step and a fine-tuned generative decoder for the second, making it highly efficient and suitable for large-scale reconstruction. With these distinct features, Scale-MIA represents a potent and inconspicuous approach to breach privacy in federated learning settings, prompting the need for robust defense mechanisms against such advanced attacks.

References

- [1] B. McMahan, E. Moore, D. Ramage, S. Hampson, and B. A. y Arcas, "Communication-efficient learning of deep networks from decentralized data," in *Artificial intelligence and statistics*. PMLR, 2017, pp. 1273–1282.
- [2] D. Enthoven and Z. Al-Ars, "An overview of federated deep learning privacy attacks and defensive strategies," *Federated Learning Systems: Towards Next-Generation AI*, pp. 173–196, 2021.
- [3] L. Zhu, Z. Liu, and S. Han, "Deep leakage from gradients," *Advances in neural information processing systems*, vol. 32, 2019.
- [4] B. Zhao, K. R. Mopuri, and H. Bilen, "idlg: Improved deep leakage from gradients," *arXiv preprint arXiv:2001.02610*, 2020.
- [5] J. Geiping, H. Bauermeister, H. Dröge, and M. Moeller, "Inverting gradients-how easy is it to break privacy in federated learning?" *Advances in Neural Information Processing Systems*, vol. 33, pp. 16 937–16 947, 2020.
- [6] J. Zhu and M. Blaschko, "R-gap: Recursive gradient attack on privacy," *arXiv preprint arXiv:2010.07733*, 2020.
- [7] H. Yin, A. Mallya, A. Vahdat, J. M. Alvarez, J. Kautz, and P. Molchanov, "See through gradients: Image batch recovery via gradinversion," in *Proceedings of the IEEE/CVF Conference on Computer Vision and Pattern Recognition*, 2021, pp. 16 337–16 346.
- [8] J. Lu, X. S. Zhang, T. Zhao, X. He, and J. Cheng, "April: Finding the achilles' heel on privacy for vision transformers," in *Proceedings of the IEEE/CVF Conference on Computer Vision and Pattern Recognition*, 2022, pp. 10 051–10 060.
- [9] A. Hatamizadeh, H. Yin, H. R. Roth, W. Li, J. Kautz, D. Xu, and P. Molchanov, "Gradvit: Gradient inversion of vision transformers," in *Proceedings of the IEEE/CVF Conference on Computer Vision and Pattern Recognition*, 2022, pp. 10 021–10 030.
- [10] K. Bonawitz, V. Ivanov, B. Kreuter, A. Marcedone, H. B. McMahan, S. Patel, D. Ramage, A. Segal, and K. Seth, "Practical secure aggregation for privacy-preserving machine learning," in *proceedings of the 2017 ACM SIGSAC Conference on Computer and Communications Security*, 2017, pp. 1175–1191.
- [11] Y. Huang, S. Gupta, Z. Song, K. Li, and S. Arora, "Evaluating gradient inversion attacks and defenses in federated learning," *Advances in Neural Information Processing Systems*, vol. 34, pp. 7232–7241, 2021.
- [12] J. H. Bell, K. A. Bonawitz, A. Gascón, T. Lepoint, and M. Raykova, "Secure single-server aggregation with (poly) logarithmic overhead," in *Proceedings of the 2020 ACM SIGSAC Conference on Computer and Communications Security*, 2020, pp. 1253–1269.
- [13] X. Guo, Z. Liu, J. Li, J. Gao, B. Hou, C. Dong, and T. Baker, "V eri fl: Communication-efficient and fast verifiable aggregation for federated learning," *IEEE Transactions on Information Forensics and Security*, vol. 16, pp. 1736–1751, 2020.
- [14] S. Kadhe, N. Rajaraman, O. O. Koyluoglu, and K. Ramchandran, "Fast-secagg: Scalable secure aggregation for privacy-preserving federated learning," *arXiv preprint arXiv:2009.11248*, 2020.
- [15] G. Xu, H. Li, S. Liu, K. Yang, and X. Lin, "Verifynet: Secure and verifiable federated learning," *IEEE Transactions on Information Forensics and Security*, vol. 15, pp. 911–926, 2019.
- [16] D. Pasquini, D. Francati, and G. Ateniese, "Eluding secure aggregation in federated learning via model inconsistency," in *Proceedings of the 2022 ACM SIGSAC Conference on Computer and Communications Security*, 2022, pp. 2429–2443.
- [17] Y. Wen, J. Geiping, L. Fowl, M. Goldblum, and T. Goldstein, "Fishing for user data in large-batch federated learning via gradient magnification," *arXiv preprint arXiv:2202.00580*, 2022.
- [18] L. Fowl, J. Geiping, W. Czaja, M. Goldblum, and T. Goldstein, "Robbing the fed: Directly obtaining private data in federated learning with modified models," *arXiv preprint arXiv:2110.13057*, 2021.
- [19] J. C. Zhao, A. Sharma, A. R. Elkordy, Y. H. Ezzeldin, S. Avestimehr, and S. Bagchi, "Secure aggregation in federated learning is not private: Leaking user data at large scale through model modification," *arXiv preprint arXiv:2303.12233*, 2023.
- [20] H. Xiao, K. Rasul, and R. Vollgraf, "Fashion-mnist: a novel image dataset for benchmarking machine learning algorithms," *arXiv preprint arXiv:1708.07747*, 2017.
- [21] N. Codella, V. Rotemberg, P. Tschandl, M. E. Celebi, S. Dusza, D. Gutman, B. Helba, A. Kalloo, K. Liopyris, M. Marchetti *et al.*, "Skin lesion analysis toward melanoma detection 2018: A challenge hosted by the international skin imaging collaboration (isic)," *arXiv preprint arXiv:1902.03368*, 2019.
- [22] R. H. Byrd, S. L. Hansen, J. Nocedal, and Y. Singer, "A stochastic quasi-newton method for large-scale optimization," *SIAM Journal on Optimization*, vol. 26, no. 2, pp. 1008–1031, 2016.
- [23] Y. Aono, T. Hayashi, L. Wang, S. Moriai *et al.*, "Privacy-preserving deep learning via additively homomorphic encryption," *IEEE transactions on information forensics and security*, vol. 13, no. 5, pp. 1333–1345, 2017.
- [24] B. Choi, J.-y. Sohn, D.-J. Han, and J. Moon, "Communication-computation efficient secure aggregation for federated learning," *arXiv preprint arXiv:2012.05433*, 2020.
- [25] K. Pillutla, S. M. Kakade, and Z. Harchaoui, "Robust aggregation for federated learning," *IEEE Transactions on Signal Processing*, vol. 70, pp. 1142–1154, 2022.
- [26] L. Burkharter, H. Lycklama, A. Viand, N. Küchler, and A. Hithnawi, "Rofl: Attestable robustness for secure federated learning," *arXiv e-prints*, pp. arXiv–2107, 2021.
- [27] D. Bank, N. Koenigstein, and R. Giryas, "Autoencoders," *arXiv preprint arXiv:2003.05991*, 2020.
- [28] Y. Pu, Z. Gan, R. Henao, X. Yuan, C. Li, A. Stevens, and L. Carin, "Variational autoencoder for deep learning of images, labels and captions," *Advances in neural information processing systems*, vol. 29, 2016.
- [29] J. An and S. Cho, "Variational autoencoder based anomaly detection using reconstruction probability," *Special lecture on IE*, vol. 2, no. 1, pp. 1–18, 2015.
- [30] M. J. Kusner, B. Paige, and J. M. Hernández-Lobato, "Grammar variational autoencoder," in *International conference on machine learning*. PMLR, 2017, pp. 1945–1954.
- [31] M. Tschannen, O. Bachem, and M. Lucic, "Recent advances in autoencoder-based representation learning," *arXiv preprint arXiv:1812.05069*, 2018.
- [32] A. Krizhevsky, G. Hinton *et al.*, "Learning multiple layers of features from tiny images," 2009.
- [33] A. Krizhevsky, I. Sutskever, and G. E. Hinton, "Imagenet classification with deep convolutional neural networks," *Advances in neural information processing systems*, vol. 25, 2012.
- [34] K. Simonyan and A. Zisserman, "Very deep convolutional networks for large-scale image recognition," *arXiv preprint arXiv:1409.1556*, 2014.
- [35] K. He, X. Zhang, S. Ren, and J. Sun, "Deep residual learning for image recognition," in *Proceedings of the IEEE conference on computer vision and pattern recognition*, 2016, pp. 770–778.
- [36] A. Dosovitskiy, L. Beyer, A. Kolesnikov, D. Weissenborn, X. Zhai, T. Unterthiner, M. Dehghani, M. Minderer, G. Heigold, S. Gelly *et al.*, "An image is worth 16x16 words: Transformers for image recognition at scale," *arXiv preprint arXiv:2010.11929*, 2020.
- [37] C. Dwork, A. Roth *et al.*, "The algorithmic foundations of differential privacy," *Foundations and Trends® in Theoretical Computer Science*, vol. 9, no. 3–4, pp. 211–407, 2014.

- [38] M. Abadi, A. Chu, I. Goodfellow, H. B. McMahan, I. Mironov, K. Talwar, and L. Zhang, “Deep learning with differential privacy,” in *Proceedings of the 2016 ACM SIGSAC conference on computer and communications security*, 2016, pp. 308–318.
- [39] H. B. McMahan, D. Ramage, K. Talwar, and L. Zhang, “Learning differentially private recurrent language models,” in *International Conference on Learning Representations*, 2018.
- [40] S. H. Na, H. G. Hong, J. Kim, and S. Shin, “Closing the loophole: Rethinking reconstruction attacks in federated learning from a privacy standpoint,” in *Proceedings of the 38th Annual Computer Security Applications Conference*, 2022, pp. 332–345.

Appendix A. FedAVG

As we have mentioned in the section 3, the federated learning system may also employ the FedAVG algorithm. The FedAVG algorithm requires the clients to train the global model G with their datasets D_i for multiple local iterations l^t in the global round t before sending back their parameter updates. This process can be expressed as $\theta_i^{(t,j+1)} = \theta_i^{(t,j)} - \eta \frac{1}{|D_i^t|} \nabla L(\theta_i^t, D_i^t)$, where $j \in \{1, 2, \dots, l^t\}$ refers to the local training iterations. After finishing this, the clients upload the model parameters $\theta_i^t = \theta_i^{(t,l^t)}$ to the parameter server and the server performs FedAVG as follows:

$$\theta^{t+1} = \sum_{i=1}^n \frac{\alpha_i}{|D_i^t|} \theta_i^t \quad (7)$$

Appendix B. Proof of Linear Leakage

We provide mathematical proofs for the following two properties of the linear leakage primitive.

Property 1: For l in $\{1, 2, \dots, k\}$, considering x_p is the p^{th} smallest sample in terms of feature $h(x)$ and falls in the l^{th} bin $[h_l, h_{l+1}]$ alone, $\nabla_{w_1(l+1)} L$ satisfies $\nabla_{w_1(l+1)} L = \frac{\partial L}{\partial y_{l+1}} \frac{\partial y_{l+1}}{\partial w_1(l+1)} = \sum_{v=1}^p \frac{\partial L}{\partial y_{l+1}} x_v$.

Proof: According to the chain rule, we can calculate the gradient as $\nabla_{w_1(l+1)} L = \sum_{v=1}^k \frac{\partial L}{\partial y_{l+1}} x_v$. We decompose this equation into two parts as $\sum_{v=1}^p \frac{\partial L}{\partial y_{l+1}} x_v + \sum_{v=p+1}^k \frac{\partial L}{\partial y_{l+1}} x_v$. For the second part, we have $y_{l+1} < 0$ because all these x_v are smaller than x_p and can not activate bin l . Then according to the property of the ReLU function (zero gradients for negative values), $\frac{\partial L}{\partial y_{l+1}} = 0$ for these values. This indicates that the second part is always zero and the property holds.

Property 2: By letting the row vectors of w_2 identical, we have $\frac{\partial L}{\partial y_{l+1}} = \frac{\partial L}{\partial y_l}$.

Proof: According to the chain rule, we have $\frac{\partial L}{\partial y_{l+1}} = \sum_{i=1}^o \frac{\partial L}{\partial z_i} \frac{\partial z_i}{\partial y_{l+1}}$. Because all the row vectors of w_2 are identical, $\frac{\partial z_i}{\partial y_{l+1}} = \frac{\partial z_i}{\partial y_l}$ for all $i \in \{1, 2, \dots, o\}$. Then we take it back and have $\sum_{i=1}^o \frac{\partial L}{\partial z_i} \frac{\partial z_i}{\partial y_{l+1}} = \sum_{i=1}^o \frac{\partial L}{\partial z_i} \frac{\partial z_i}{\partial y_l} = \frac{\partial L}{\partial y_l}$.

Appendix C. Batched Reconstruction Examples

We plot three randomly selected reconstructed batches with batch size 64 for the CIFAR-10, FMNIST, and HMNIST datasets in Figure 7, Figure 8, and Figure 9 respectively. For each figure, we plot the original input batch on the left and the reconstructed results on the right. We can observe excellent recovery performance on all three batches.

TABLE 9. CNN NETWORK ARCHITECTURE.

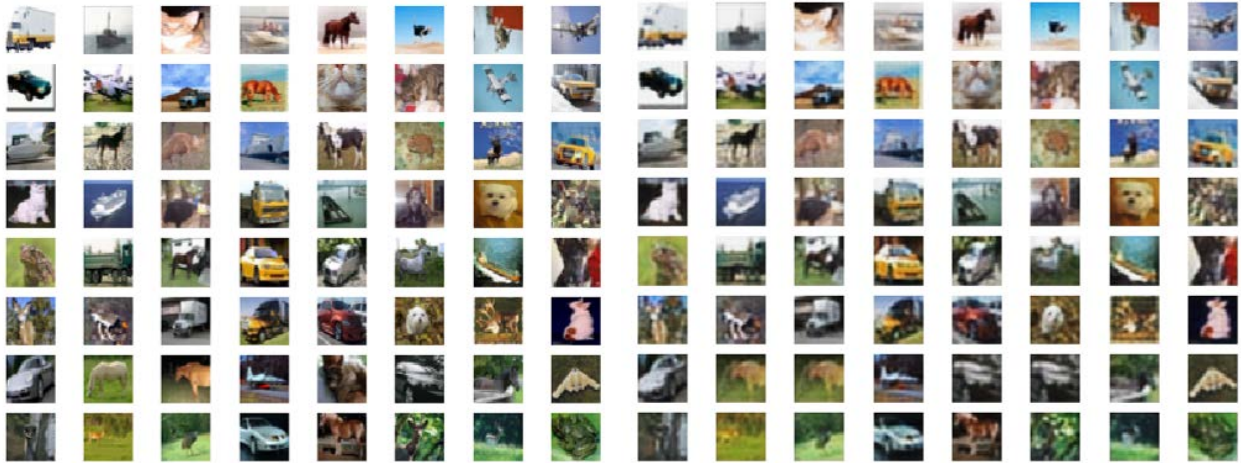
	Sizes	Filter	Stride, Padding	Activation
Input	$32 \times 32 \times 3$	/	/, /	/
conv2d_1	$16 \times 16 \times 12$	$12 \times 4 \times 4$	2, 1	ReLU
conv2d_2	$8 \times 8 \times 32$	$32 \times 4 \times 4$	2, 1	ReLU
conv2d_3	$4 \times 4 \times 64$	$64 \times 4 \times 4$	2, 1	ReLU
flatten_1	$4 \times 4 \times 64$	/	/	/
dense_1	1024	/	/	ReLU
dense_2	512	/	/	ReLU
dense_3	10	/	/	ReLU

TABLE 10. ALEXNET NETWORK ARCHITECTURE.

	Sizes	Filter	Stride, Padding	Activation
Input	$32 \times 32 \times 3$	/	/, /	/
conv2d_1	$32 \times 32 \times 64$	$64 \times 3 \times 3$	1, 1	ReLU
maxpool2d_1	$16 \times 16 \times 64$	$64 \times 2 \times 2$	/	/
conv2d_2	$16 \times 16 \times 192$	$192 \times 3 \times 3$	1, 1	ReLU
maxpool2d_2	$8 \times 8 \times 192$	$192 \times 2 \times 2$	/	/
conv2d_3	$8 \times 8 \times 384$	$384 \times 3 \times 3$	1, 1	ReLU
conv2d_4	$8 \times 8 \times 256$	$256 \times 3 \times 3$	1, 1	ReLU
conv2d_5	$8 \times 8 \times 256$	$256 \times 3 \times 3$	1, 1	ReLU
maxpool2d_3	$4 \times 4 \times 256$	$256 \times 2 \times 2$	/	/
flatten_1	$4 \times 4 \times 256$	/	/	/
dense_1	512	/	/	ReLU
dense_2	120	/	/	ReLU
dense_3	10	/	/	ReLU

Appendix D. Neural Network Architectures

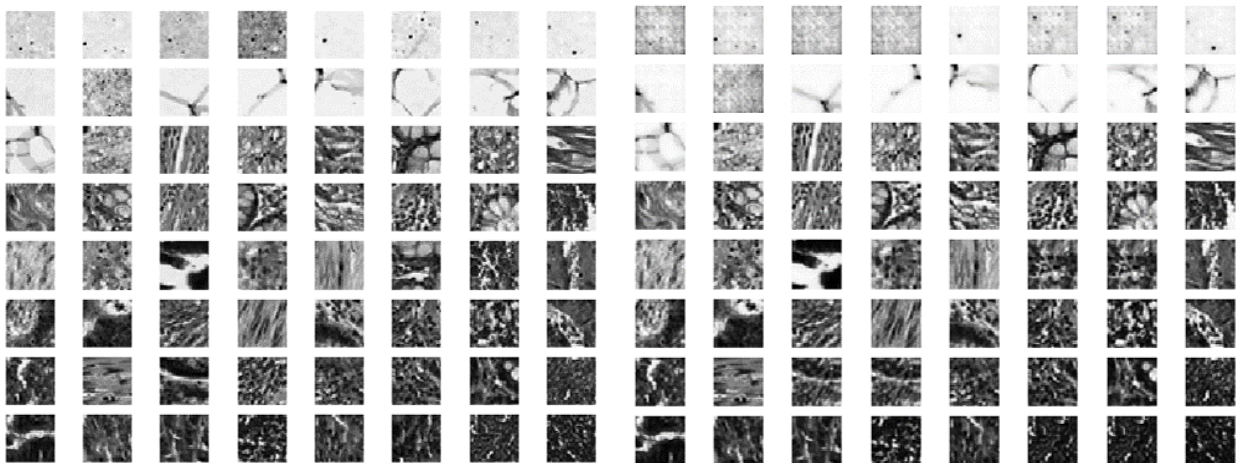
We demonstrate the model architectures in section 6 including the CNN, Alexnet, Resnet, and VGGnet in Table 9 to Table 12 respectively. We also demonstrate the network architecture configurations for ViT in Table 13. For all models, we take the CIFAR-10 as the input dataset and demonstrate their feature map sizes, kernel sizes, stride/padding values, and activation functions.



(a) A batch of 64 figures from the CIFAR-10 dataset. (b) The reconstructed figures for the CIFAR-10 dataset.
Figure 7. The comparison between the original figures and the reconstructed figures with batch size 64 on CIFAR-10.



(a) A batch of 64 figures from the FMNIST dataset. (b) The reconstructed figures for the FMNIST dataset.
Figure 8. The comparison between the original figures and the reconstructed figures with batch size 64 on FMNIST.



(a) A batch of 64 figures from the HMnist dataset. (b) The reconstructed figures for the HMnist dataset.
Figure 9. The comparison between the original figures and the reconstructed figures with batch size 64 on HMnist.

TABLE 11. VGGNET NETWORK ARCHITECTURE.

	Sizes	Filter	Stride, Padding	Activation
Input	$32 \times 32 \times 3$	/	/, /	/
conv2d_1	$32 \times 32 \times 64$	$64 \times 3 \times 3$	1, 1	ReLU
maxpool2d_1	$16 \times 16 \times 64$	$64 \times 2 \times 2$	2, 0	/
conv2d_2	$16 \times 16 \times 128$	$128 \times 3 \times 3$	1, 1	ReLU
maxpool2d_2	$8 \times 8 \times 128$	$128 \times 2 \times 2$	2, 0	/
conv2d_3	$8 \times 8 \times 256$	$256 \times 3 \times 3$	1, 1	ReLU
conv2d_4	$8 \times 8 \times 256$	$256 \times 3 \times 3$	1, 1	ReLU
maxpool2d_1	$4 \times 4 \times 512$	$256 \times 2 \times 2$	2, 0	/
conv2d_5	$8 \times 8 \times 512$	$512 \times 3 \times 3$	1, 1	ReLU
conv2d_6	$8 \times 8 \times 512$	$512 \times 3 \times 3$	1, 1	ReLU
maxpool2d_1	$4 \times 4 \times 512$	$512 \times 1 \times 1$	1, 0	/
conv2d_7	$4 \times 4 \times 512$	$512 \times 3 \times 3$	1, 1	ReLU
conv2d_8	$4 \times 4 \times 512$	$512 \times 3 \times 3$	1, 1	ReLU
maxpool2d_1	$4 \times 4 \times 512$	$512 \times 1 \times 1$	1, 0	/
avgpool2d_1	$4 \times 4 \times 512$	$512 \times 1 \times 1$	1, 0	/
flatten_1	$4 \times 4 \times 512$	/	/	/
dense_1	1024	/	/	ReLU
dense_2	200	/	/	ReLU
dense_3	10	/	/	ReLU

TABLE 12. RESNET NETWORK ARCHITECTURE.

	Sizes	Filter	Stride, Padding	Activation
Input	$32 \times 32 \times 3$	/	/, /	/
conv2d_1	$32 \times 32 \times 32$	$64 \times 3 \times 3$	1, 1	ReLU
conv1_x	$32 \times 32 \times 32$	$32 \times 3 \times 3$	2, 1	ReLU
		$32 \times 3 \times 3$	1, 1	ReLU
conv2_x	$16 \times 16 \times 64$	$64 \times 3 \times 3$	2, 1	ReLU
		$64 \times 3 \times 3$	1, 1	ReLU
conv3_x	$8 \times 8 \times 128$	$128 \times 3 \times 3$	2, 1	ReLU
		$128 \times 3 \times 3$	1, 1	ReLU
conv4_x	$4 \times 4 \times 256$	$256 \times 3 \times 3$	2, 1	ReLU
		$256 \times 3 \times 3$	1, 1	ReLU
avgpool2d_1	$4 \times 4 \times 256$	$256 \times 1 \times 1$	/	/
flatten_1	$4 \times 4 \times 256$	/	/	/
dense_1	512	/	/	ReLU
dense_2	10	/	/	ReLU

TABLE 13. ViT NETWORK CONFIGURATIONS.

Configurations	Values
Image size	32
Patch size	8
Number of classes	10
Dimension	512
Depth	6
MLP dimension	512
Heads	8